2016-04-01

Numerical simulation and experimental verification of heating performance of an integrally water-heated tool

Abdalrahman, R

10.1177/0731684415626804
Journal of Reinforced Plastics and Composites
SAGE

Numerical Simulation and Experimental Verification of Heating Performance of an Integrally Water-heated Tool

Rzgar Abdalrahman[a]*, Stephen Grove[b], Adam Kyte[b], Md Jahir Rizvi[b]

[a] Mechanical Engineering Department, Polytechnic University of Slemani, Slemani, Iraq
[b] School of Marine Science & Engineering, Plymouth University, Plymouth, UK PL4 8AA
*Corresponding Author: rzgar.abdalrahman@plymouth.ac.uk

Keywords: composite, tool manufacturing, thermal property measurement, numerical simulation, verification.

ABSTRACT

Design and manufacturing of composite tooling is crucial in producing cost effective composite components with high quality. Aimed at identifying the optimal design of integrally heated tools in terms of their thermal performance, a number of design variables were investigated numerically in a previous study by Abdalrahman et al. (2014). Statistical analysis of the simulation results revealed that a parallel layout of heating channels can significantly improve the heating performance, and channel separation should be determined according to the production requirement. In the present work, an integrally water-heated tool is manufactured according to the optimal design after some geometry amendments. Thermal properties of the constituent materials of the produced tool are also measured. A numerical model of the tool geometry is simulated with actual material properties and boundary conditions to calculate the response variables of temperature uniformity and heating rate. The numerical results are verified by experimental testing, using a thermal camera and thermocouples. Good agreement between the simulation and the experimental results confirmed the suitability of numerical simulation in predicting the thermal performance of integrally-heated tooling and the validity of the boundary conditions.

Nomenclature

Symbols		Discerptions	Units
c_p	:	Specific heat capacity	J/kg.K
D_h	:	Hydraulic diameter of channel	m
g	:	Acceleration due to gravity	m/s^2
h	:	Heat transfer coefficient of fluid	$W/m^2.K$
h_t	:	Heat transfer coefficient of top face	$W/m^2.K$
H_t	:	Experimental heating time of the tool heated by hot inlet water	min
H_{t_c}	:	Experimental heating time of the tool heated from cold	min
H_{t_s}	:	Numerically-calculated heating time	min
k	:	Thermal conductivity	W/m.K
L	:	Length of the surface	m
L_o	:	Length of top or bottom faces	m
$\Delta p_1, .., \Delta p_4$	:	Pressure drops in the parallel branches	Pa ($kg/m.s^2$)
Pr	:	Prandtl number $(c_p\mu/k)$	-
Q	:	volumetric flow rate in the main inlet	m^3/min (L/min)
$Q_1, ., Q_4$	:	volumetric flow rate in the parallel branches	m^3/min (L/min)
Ra_L	:	Rayleigh number	-
$\mathrm{Re_D}$	:	Reynold's number of channel flow $(\rho u D_h/\mu)$	-
R_i	:	Ratio of pipe length to its diameter	-
T_A	:	Absolute temperature	K
T_a	:	Fluid wall temperature	^{o}C
T_{f_a}	:	Air film temperature	^{o}C
T_m	:	Maximum temperature of the mould	^{o}C
T_{m_i}	:	Initial temperature of mould face	^{o}C
T_{m_m}	:	Mould mean temperature	^{o}C
T_∞	:	Ambient temperature	^{o}C
u	:	Fluid velocity	m/s
W_{H_t}	:	Water heating time (from hot connection)	min
$W_{H_{t_C}}$	:	Water heating time (from cold connection)	min
α	:	Coefficient of thermal expansion	K^{-1}
$\propto$	:	Thermal diffusivity	m^2/s
ρ	:	Density	kg/m^3
μ	:	Dynamic viscosity	$N.m/s^2$ kg/m.s

1 Introduction

Recently, different innovative approaches have been developed to overcome the problems of traditional methods of composite manufacturing e.g. high operating costs, energy losses and long curing times. These disadvantages are particularly associated with the use of autoclaves. One of the technologies that can produce composite components without an autoclave is the integrally-heated-tool, and is widely used in different industries, such as wind energy, aerospace and surface transport (Marsh, 2003; Mason, 2006). This is because integrally heated-tools enable fabrication of large components with complex shapes and can overcome the size limitation problems of ovens and autoclaves and their significant consumption of heat energy, time and capital (Arney et al., 2004; Raizenne, Hind & Poupore, 2006; Walczyk & Kuppers, 2012).

The heating unit in the integrally-heated-tools directly attaches to the tool and eliminates the need for heating the surrounding environment, hence increasing the heating rate and saving energy (Baril-Gosselin, 2013; Raizenne, Hind & Poupore, 2006). According to the installation, the heating unit may be attached to the tool externally or embedded (Black, 2011). Heating is achieved by circulating a hot fluid in pockets connected directly to the tool or in a channel embedded in it (Yao, Chen & Kim, 2008). This method is widely used in the composite industry, and in plastic injection moulding and thermoforming processes due to its advantages compared to electrical heating techniques (Marsh, 2003). The preferred heating medium is water because it is a low cost and efficient heating medium, requiring minimum power for heating and pumping due to its low viscosity and high thermal capacity, and the achieved temperature never exceeds required tool surface temperature (Marsh, 2003). Water can also be used for cooling.

Various studies have compared the heating performance of different fluids, e.g. oil, water, steam, pressurised water, as well as other heating techniques such as electric cartridge, electric resistive, oven and infrared induction (Black, 2010b; Petrykowski & Fischer, 2012; PMC; Sloan, 2013). Results have shown that water is superior in achieving the desired temperature over the mould face uniformly with the lowest cost, time and consumed energy. Most of the tool's physical, thermal and mechanical characteristics depend on the tool material (Murphy, 1998; Rosato, 2004; Scott Bader Company, 2005). Composite materials, compared to metals, can offer the advantages of low manufacturing cost and time as well as low coefficients of thermal expansion (CTE). The key problem of composite tools is their low thermal conductivity, especially through-thickness; this is mainly due to the polymer matrix, the conductivity of which could be improved by adding filling materials (Milella et al., 2014).

In order to improve the heating performance of an integrally water heated tool, the effects of a number of design variables, e.g. shape, layout and separation of heating channels, were investigated numerically by Abdalrahman et al. (2014) based on the following assumptions:

- The temperature of water entering the tool was assumed to be constant at its maximum possible temperature of 90^{o}C, which results in a constant thermal boundary condition at the model inlet. This boundary condition could be achieved practically in industry with established adequate resources as mentioned by Ding et al.(2001).
- A free air convection boundary condition was assumed at the top, bottom and side surfaces of the tool model.

It was concluded that a parallel layout of heating channels significantly improved the performance of the tool compared to the other geometries studied. Reducing the channel separation in the composite tooling, unlike in high thermal conductivity metallic tooling, does not improve the temperature uniformity over the tool face, due to its low thermal diffusivity. Therefore the channel separation should be determined according to the production requirements of the component produced by the tool.

In the current study an experimental tool is built according to the predicted optimal design, after some minor amendments to the channel separation and number of the parallel channels to increase the tool surface area and facilitate the tool manufacturing and temperature measurement. Tooling materials of carbon fibre reinforced epoxy (CFRP) laminate and Alepoxy (aluminium powder/epoxy composite) are selected according to their availability and cost for constructing the tool face and the mould, respectively. The tool is manufactured with an integrated method that can provide good contact between the tool parts and eliminate the problems of production (e.g. void content, resin richness, residual strain and low volume fraction) as much as possible. The tool materials are tested practically to measure their diffusivity, specific heat and conductivity. The produced optimal tool (after amendment) is simulated in ANSYS software to explore its thermal performance with regard to heating time and surface temperature uniformity. Finally the produced tool is tested experimentally defining its practical thermal performance and verifying the numerical results. Calibrated measurement apparatus (thermal camera, thermocouples and a flowmeter) are used during the experiments. Results show good agreement between calculation and experiment, confirming the suitability of numerical simulation in predicting the optimal designs of integrally heated tool and appropriate assignment of the boundary conditions.

2 Literature review

Integrally heated tooling is an alternative to the conventional methods of composite fabrication that can offer the following benefits for composite manufacturing, compared to traditional methods (Arney *et al.*, 2004; Raizenne, Hind & Poupore, 2006; Walczyk & Kuppers, 2012).

- Heating the composite parts more directly, during curing.
- Fabricating large and complex shape components.
- Consuming lower amounts of heat (energy), time and capital.

The technology can be used in all process variations of vacuum bagging (VB), resin infusion (RI) and resin transfer moulding (RTM). Compared to traditional methods, integrally heated tools can save energy and reduce cure times by approximately 40% by increasing heating rates up to 5 $^{\circ}$C/min (Baril-Gosselin, 2013; Raizenne, Hind & Poupore, 2006). This is because the heating source, in the integrally heated tools, is directly attached to the tool (either connected to the tool externally or embedded during manufacture) and eliminates the need for heating the surrounding environment (Black, 2011).

Progoulakis (2004) prepared cost data, as listed in Table 1, for a comparison of an integrally heated tool with autoclave and oven for manufacturing a 12 m long composite C beam by resin film infusion, and concluded that the heated tool reduced the estimated power requirements, operating and equipment procurement costs, except that of the procurement. Also he deduced that integrally heated tool offers a 15% reduction in manufacturing risk of

potential damage to tooling equipment and components because it does not require a frequent move in and out of autoclave and oven.

Table 1 Cost data and performance comparison of processing options (Progoulakis, 2004).

Cost Data	unit	Heated tool	Autoclave	oven
Estimated power requirements	kW	30	720	150
Operating cost	£/h	3	10	7.5
Procurement costs	£	15,000	475,000	85,000
Pre-production requirements costs	£	72,000	63,000	63,000
Production requirements costs (capital investment)	£	2,080,000	2,540,000	2,150,000

Different materials such as steel, aluminium, Invar, Nilo, monolithic graphite, ceramics, E-glass and carbon fibre prepreg have been used as tool materials in the composite industry (Campbell, 2004; Kruckenberg & Paton, 1998 ; Mazumdar, 2001). Selection of the proper tool material depends on the manufacturing process in which the tool is used and the production runs. The preference for composites over the other tooling materials is due to their low coefficient of thermal expansion (CTE) which matches that of the components and thereby decreases the development of residual stresses, distortion and dimensional inaccuracies. Another advantage of composite tools, especially CFRP, is that they have lower weight and thermal inertia compared to metallic tools. Although Invar and Nilo have low CTEs, they have a high thermal inertia (low heating/cooling rates) in addition to high purchasing and processing costs (Campbell, 2004).

In the current study CFRP is selected because it can provide high wear resistance and strength as well as low weight and thermal expansion. However, CFRP composites have relatively low through-thickness thermal conductivity, due to the absence of fibres in this direction and the presence of a polymer-rich interface between the lamellae (Han & Chung, 2011; Han et al., 2008). The through-thickness thermal conductivity of carbon fibre composites can be enhanced by using three-dimensionally woven fabrics, the incorporation of fillers and moulding at high curing pressure to achieve a higher volume fraction (Schuster et al., 2008; Schuster et al., 2009) During a study for improving through-thickness thermal conductivity of CFRP composites, Gallagher (2012) applied a heterogeneously structured resin with conductive silver filler and obtained a thermal conductivity in excess of 5 W/m.K with 9% weight fraction of silver.

Aluminium particles-epoxy resin composite (Alepoxy) can offer manufacturing flexibility (Zweben, 1998), facilitate embedding the heating channels and provide a coherent joint with both the channel and the tool face laminate, and is therefore used in the current study. Senthilkumar et al. (2012) concluded that Alepoxy with 0.5 volume fraction provides 4.67 W/m.K thermal conductivity, while Tomlinson and Stapley (1977) measured 1.35 W/m.K. The variation may be due to the difference of resin type, particle size and/or measurement methods used. Furthermore Zhou & Yu (2010) concluded that the thermal conductivity of Alepoxy is influenced by the size, concentration and surface modification of the particles, e.g. composites of 2 μm particles with 0.48 volume fraction has thermal conductivity of 1.25 W/m.K while that of 40 μm has 1.16 W/m.K. They also noted that uniform dispersion of the particles eliminates agglomeration and decreases air voids.

3 Overview of the experimental heated-tool

3.1 Tool design

The experimental tool was based on the first optimal combination predicted in a previous theoretical study, in which an optimal combination of design variables was found to be a parallel layout of heating channels, rectangular tube profile and 36 mm channel separation, considering the response variable of heating time per unit mass (Abdalrahman *et al.*, 2014). The following minor amendments were made:

- The channel separation was increased by 4 mm to facilitate the channel connection during manufacturing.
- Circular instead of rectangular channels were selected as they are readily available. This was found to have very little influence on heating efficiency.

The width of the optimal experimental tool depends on the channel separation (40 mm) and accordingly the effective heated zone of the CFRP tool face is a rectangle of 320 x 500 mm located directly over the mould. The main transverse pipes remain outside the mould to eliminate their effect in heating the tool face, which is achieved only by the parallel branches. The back and side faces of the tool as well as the exposed parts of the piping system are insulated completely by PVC foam in a wooden box to prevent heat loss, as shown in Figure 1.

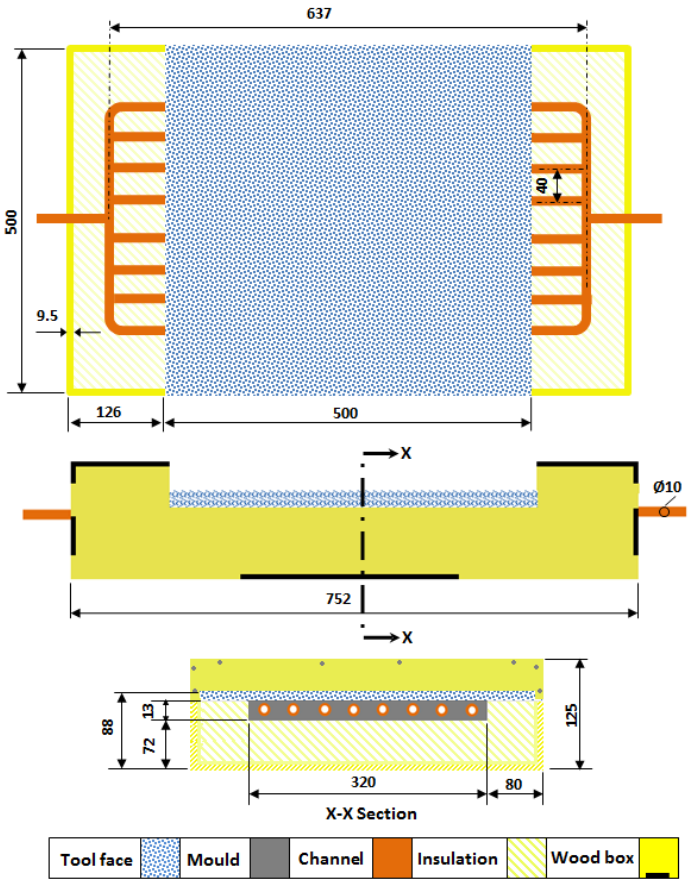

Figure 1 Dimensions (mm) of the optimal experimental tool

3.2 Tool building

The tool consists three main parts; two of them (the tool face and the channel or piping system) are initially combined temporarily in a special fixture that facilitates in situ casting of the third part (the mould). Two composite combinations of CFRP laminate and Alepoxy mixture are selected for the tool construction due to their availability and cost.

3.2.1 Piping system (Channels)

Copper pipes of 10 mm outside diameter and 0.7 mm wall thickness are used due to their availability, ease of forming and compatibility with the inlet and outlet of the heating unit. The eight parallel branches are joined by soldering to the main transverse outlet and inlet, using T and elbow joints. The piping system was built and tested initially with regard to its heating performance and leakage. The actual average flow rate, at the main inlet, was measured by a calibrated flowmeter at 75°C to be 15.68 l/min (4.5 m/s). Then the flow rate (fluid velocity) in each parallel branch, as listed in Table 2, is calculated from the total average flow rate according to equations of continuity and pressure drop equality, as follows (Munson, 2010):

$$\Delta p_1 = \Delta p_2 = \Delta p_3 = \Delta p_4 \qquad (1)$$

$$Q = Q_1 + Q_2 + Q_3 + Q_4 \qquad (2)$$

Table 2 Flow rates and Reynolds' numbers in the channel branches of the experimental tool

Channel No.	Units	Main Inlet	Outer channels	Middle channels		Inner channels
			1 & **8**	**2** & **7**	**3** & **6**	**4** & **5**
Flow rate	l/min	15.68	2.12	2.00	1.90	1.82
Fluid velocity	m/s	4.5	0.52	0.55	0.57	0.61
Reynolds No.	-	117,989	13,634	14,421	14,945	15,994

The channel length of 637 mm ensures more equal flow rates and flow profiles in the parallel branches; the maximum difference between the flow rates is 0.3 l/min and the flow rate in each channel creates turbulent flow with Reynolds number higher than 10^4. Figure 2 illustrates the assembly detail of the produced experimental tool parts.

3.2.2 Tool face

The CFRP tool face is laid up with non-crimp fabric (NCF) triaxial carbon (0, ±45) of 660 g/m^2 areal weight (Sigmatex, 2014), in a multi-axial lay-up configuration. The matrix is the two component infusion epoxy system SR8100 with SD8824 standard hardener (Sicomin Composites, (2013). The final laminate thickness is 3.1 mm, which can provide the desired strength with lower thermal resistance, as discussed in Abdalrahman et al. (2014). Finally the edges of the CFRP laminate are trimmed to obtain a square plate of side 500 mm.

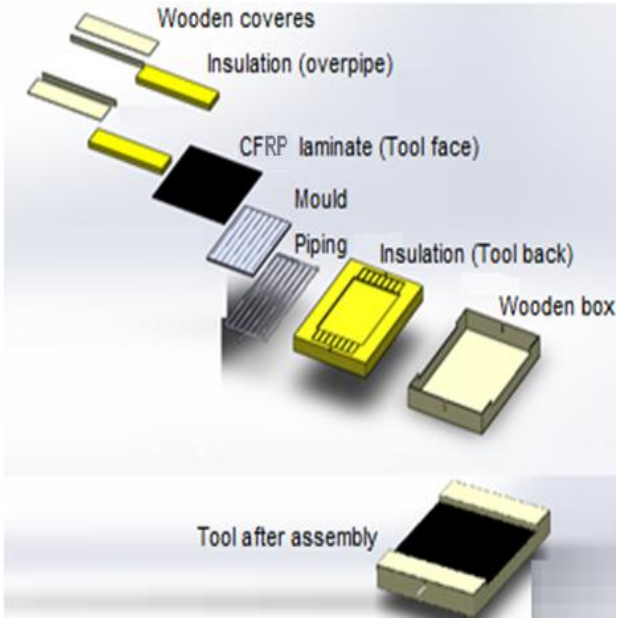

Figure 2 The assembly sequence of the experimental tool parts

3.2.3 Mould

Alepoxy particulate composite is used in manufacturing the mould, using 250 µm aluminium particles (East Coast, 2013), while the epoxy system is SR8500 with ultra-slow hardener SD8601 (Sicomin Composites, (2013).

Thermal conductivity increases with particle volume fraction (Konzelmann et al., 2008; Tomlinson & Stapley, 1977; Zhu et al., 2013). The highest volume fraction that could be easily cast into the die cavity was determined experimentally as 0.48; this mixture was prepared and cast into the fixture cavity, as shown in Figure 3, to form the mould that integrates with the channel and joins permanently to the tool face.

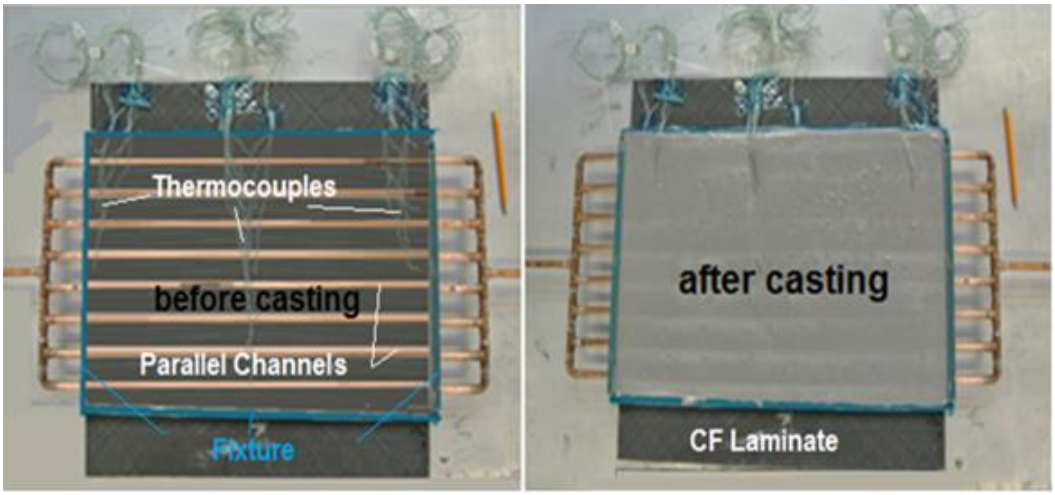

Figure 3 Combining the tool parts (with embedded thermocouples) in the fixture.

Before casting the mould, 30 K-type thermocouples, as shown in Figure 3, are distributed at the interfaces between the mould, tool face and the channel as well as the mould back face.

3.3 Material properties

The physical and thermal properties of the composite materials used, as listed in Table 3, were determined with a variety of advanced standard methods and calibrated measurement techniques.

Table 3 Calculated physical and thermal properties of the tool materials *****(Davis, 2001)

Material		W_f	V_f	ρ	c_p	$\propto$	k
		-	-	kg/m^3	J/kg.K	10^{-7} m^2/s	W/m.K
CF	(In-plane)	0.64	0.53	1500	966	-	3.00
	(out-of-plane)	0.64	0.53	1500	966	4.2	0.60
Alepoxy	(Isotropic)	0.69	0.48	1917	943.9	8.1	1.5
Copper*	(Isotropic)	-	-	8933	385	1166	401

3.3.1 Density, volume and weight fractions

The digestion method is applied to calculate the actual fibre weight in the samples of the produced CFRP laminate according to the GKN document LTI/CHEM/037 (2003) and British standard BS 7658 (1995). Densities of the applied materials are measured via water displacement (buoyancy) method according to ASTM D792-13 (2013).

3.3.2 Concentration of Al particles through the mould thickness

The particles in a viscous liquid settle down due to gravity as mentioned by Murisic et al. (2013). This phenomenon also occurs during the cure of particulate composites (e.g. Alepoxy) and causes uneven distribution of the particles through the mould thickness that may affect its properties, especially thermal conductivity. Therefore the concentration of the aluminium particles across the thickness of a specimen of the mould material (Figure 4) was inspected by scanning electron microscopy (SEM). The inspection results indicated that the area fraction of the particles, changes slightly through the mould thickness from 47% at the mould bottom to 49.5% at the top. This small difference does not have significant effect on the mould out-of-plane thermal conductivity. Consequently properties of the Alepoxy mould are assumed to be isotropic and homogeneous in the current study.

3.3.3 Thermal diffusivity

Thermal diffusivity defines the speed of heat propagation through materials (Gallagher, 2012). Thermal diffusivities of the tool materials are measured by laser flash method, using Nanoflash-xenon apparatus, type 1xLFA 447 (Netzsch), calibrated according to the ASTM E-1461-11 standard. The test was performed at the mechanical engineering laboratories at the University of Portsmouth, UK. The in-plane diffusivity of the CFRP laminate is difficult to measure because the laminate is too thin for preparing the standard square (12.7 mm) specimens.

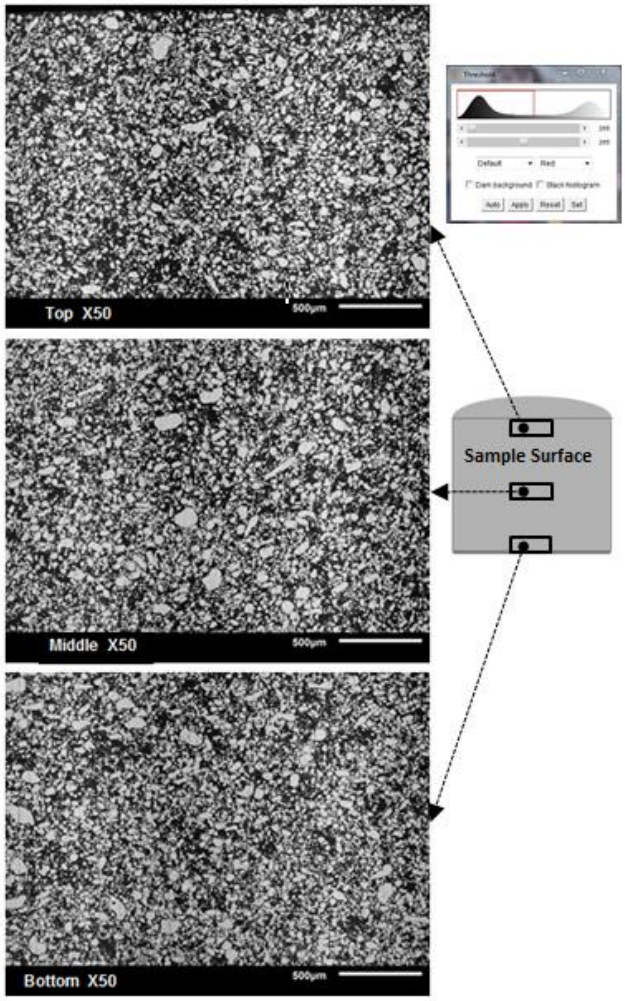

Figure 4 Aluminium particle concentration in the Alepoxy mixture, magnification is X50

3.3.4 Specific heat capacity

Differential Scanning Calorimetry (DSC), as mentioned by Cassel et al. (2012), is used to measure the specific heat according to ASTM E2716 - 09 (2014).

3.3.5 Thermal conductivity

Thermal conductivities of the isotropic Alepoxy mixture and the CFRP laminate (through-thickness) are obtained from the following equation

$$k = \rho \propto c_p \qquad (3)$$

Where the density, thermal diffusivity and specific heat are measured experimentally. The in-plane diffusivity of the orthotropic CFRP laminate is not easy to measure, therefor the in-plane thermal conductivity of the laminate was determined by ROM depending on the calculated out-plane thermal conductivity and that of the fibre reinforcement (21.6 W/m.K), was taken from literature (MatWeb, 2014).

4 Numerical simulation of the experimental tool

Due A numerical model of the experimental tool was created to investigate the performance (heating time and temperature uniformity) over the tool face. The desired operating temperature is 90ºC, but as this temperature is approached asymptotically, an arbitrary target temperature of 81ºC was used for comparison.

4.1 Tool modelling

Using symmetry, a quarter of the experimental tool geometry (Figure 5) is modelled in ANSYS Workbench. The model was meshed with 3.1 x 10^5 elements; the mesh quality was evaluated through the available metric functions of the software.

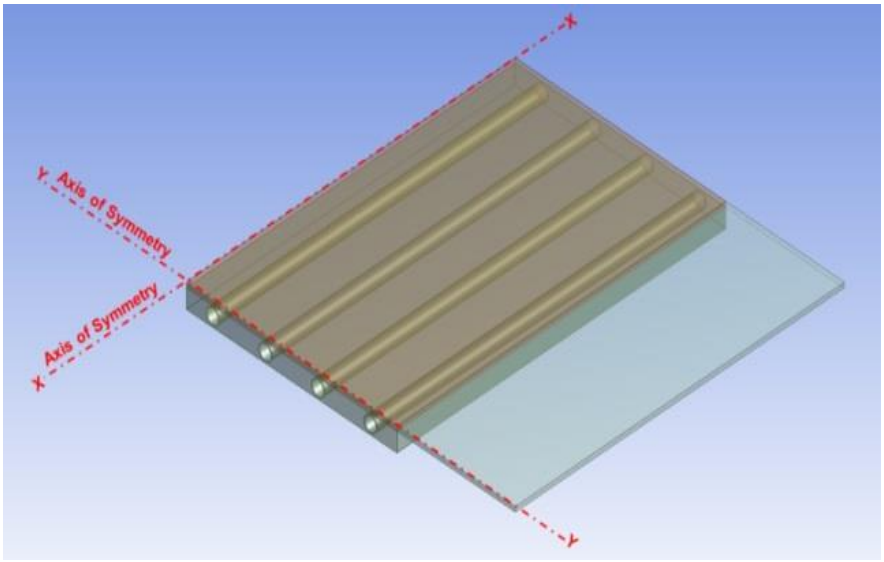

Figure 5 Geometry of the simulated part of the basic tool design

4.2 Boundary condition

The actual thermal properties of the tool materials were set according to the values in (Table 3). The inner surfaces of the channel branches were set as convection boundaries, in contact with the circulating water at 90ºC. According to the flow rate in each channel (Table 2) and the properties of water at 90ºC (Holman, 2002), the Reynolds number in all channels is higher than 10^4. Therefore the heat transfer coefficient can be calculated (Table 4) according to the empirical expression of Dittus and Boelter cited in Holman (2002).

$$\text{Where } Re_D \geq 10^4 \qquad h = 0.023\, Re_D^{0.8} Pr^{0.4} \frac{k}{D_h} \qquad (4)$$

$$Re_D = \frac{\rho u D_h}{\mu}$$

Table 4 Experimental flow rates and water heat transfer coefficient in the parallel channels of case 1, at 90°C

Channel No.	u	Re_D	h
	m/s	-	(W/m^2.K)
1 (Outer)	0.52	13634	4815
2	0.55	14421	5036
3	0.57	14945	5182
4 (Inner)	0.61	15994	5471

Free air convection is assumed at the tool face, but other faces are assumed to be adiabatic; in practice they are insulated with 75 mm of PVC foam. With ambient temperature 17°C, the mean mould and the air film temperatures are 53.5°C and 35°C respectively, according to the following equations (Incropera & DeWitt, 1996; Yoo & Walczyk, 2007).

$$T_{f_a} = \frac{T_{m_m} + T_\infty}{2} \tag{5}$$

Where $T_{m_m} = \frac{T_m + T_{m_i}}{2}$

So the properties of air are taken at 35°C from Holman (2002). Since the Rayleigh number is between than 10^4 and 10^9, the heat transfer coefficient into air, at the tool surface, is 5.7 W/m^2.K, obtained from(Holman, 2002).

$$Ra_L = \left(\frac{g\alpha(T_a - T_\infty)L^3}{\upsilon^2}.Pr\right) = \frac{g\alpha(T_a - T_\infty)L^3}{\upsilon\propto} \tag{6}$$

Where $\alpha = \frac{1}{T_A}$ for ideal gases

At the top surface, when $10^4 \leq Ra_L \leq 10^9$ $h_t = 1.32\left(\frac{T_{m_m} - T_\infty}{L_o}\right)^{0.25}$ (7)

4.3 Time step (Time scale)

The time step required for the simulation is the smaller of the convection and thermal diffusion timescales. These are calculated for transient conditions as follows, assuming a pipe length to diameter ratio of 70:

$$\text{Convective time scale} = \frac{R_i D_h}{u} \tag{8}$$

If the flow is turbulent, the thermal time scale is

$$\text{Thermal time scale} = \frac{D_h^2}{100(k/\rho c_p)} \tag{9}$$

So the calculated thermal time scale will be 0.3 s which is the smaller of the two. As the total computation time is a function of time step size, various tests were conducted with different

sizes of time step (larger than that calculated) in order to define a time step which can achieve the same simulation results with a shorter running time. A value of 1s was ultimately used.

4.4 Simulation results

The numerically-calculated temperatures at the 'slowest' corner and the centre of the heated area at the tool face are plotted in Figure 6. For comparison, the 'heating time' is defined as the time to reach a target temperature of 81ºC; this and the corresponding heating time per unit tool mass are listed in Table 5.

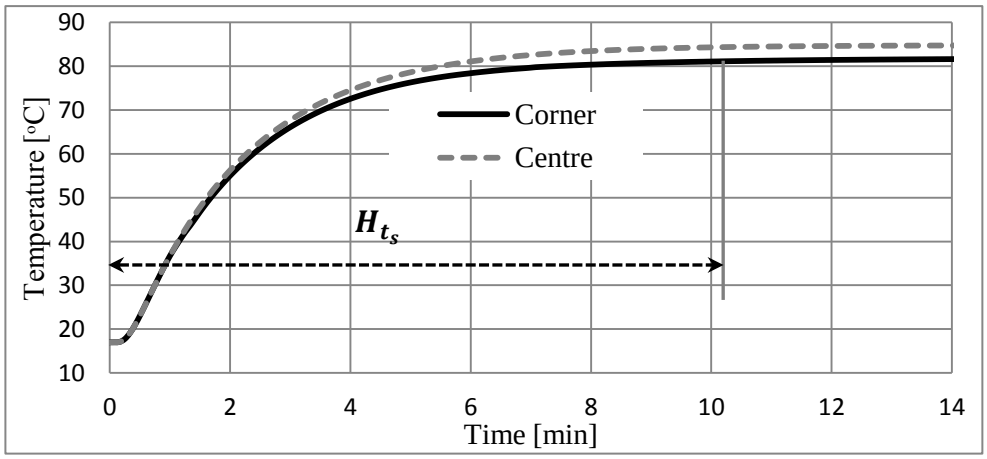

Figure 6 Numerical heating curves of the centre and slowest corner at the surface of the experimental tool model.

Figure 7A and B show the temperature distribution over the whole (heated and extended) parts of model tool surface and the heated part only, after the defined heating time, indicating that the maximum temperature over the tool face is 86.2°C. Figure 7B also shows temperature decreasing zone near the edges of the heated part that starts from the slowest heated point reached 81ºC.

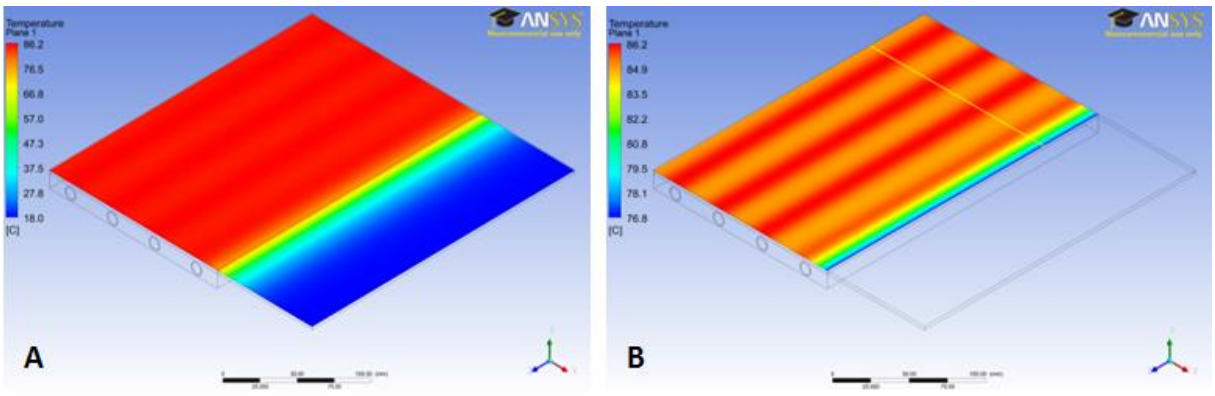

Figure 7 Temperature distribution over the model tool surface, after 10.3 min heating. **A**: whole surface. **B**: the heated part of the surface.

Temperature distribution along the width of the heated part of the tool model face (the yellow line in Figure 7B) is plotted in Figure 8. The thermal performance obtained from the numerical results is compared in Table 5.

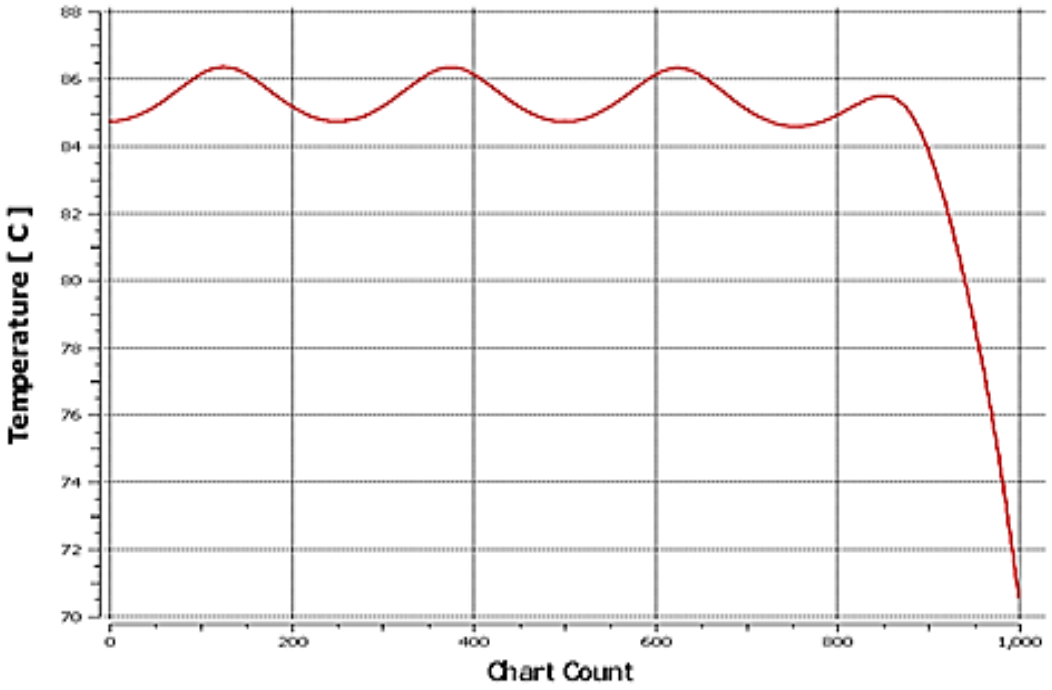

Figure 8 Temperature distribution along the half width of the heated part of the model tool surface, after 10.3 min heating

5 Experimental work

5.1 Test rig construction

The experimental test rig (Figure 9) consists of the tool connected to a heating unit that has a temperature controller TT-188, type B-0558 produced by Switzerland Tool-Temp Company. The unit is designed to heat water up to 90°C with power capacities of 3 kW, 6 kW and 9 kW. It contains a 6 litre filling tank and a centrifugal pump that can provide a maximum flow rate of 75 l/min at 4.5 bar pressure. The test rig also includes a flowmeter to measure the total actual flow rate at the main tool inlet, which is connected temporarily due to its temperature limitation (up to 80°C).

The basic three parts of the test rig are connected temporarily by plastic tubes of 10 mm outside diameter. A USB-TC data acquisition (DAQ) system with eight input channels is applied to record thermocouple outputs. As well as the permanent embedded thermocouples at the interfaces (Section 3.2.3), some others are joined temporarily to the inlet, outlet and the tool surface centre and corners. An infrared camera is installed vertically over the tool face to monitor and measure the temperature of the tool surface through thermal images capture.

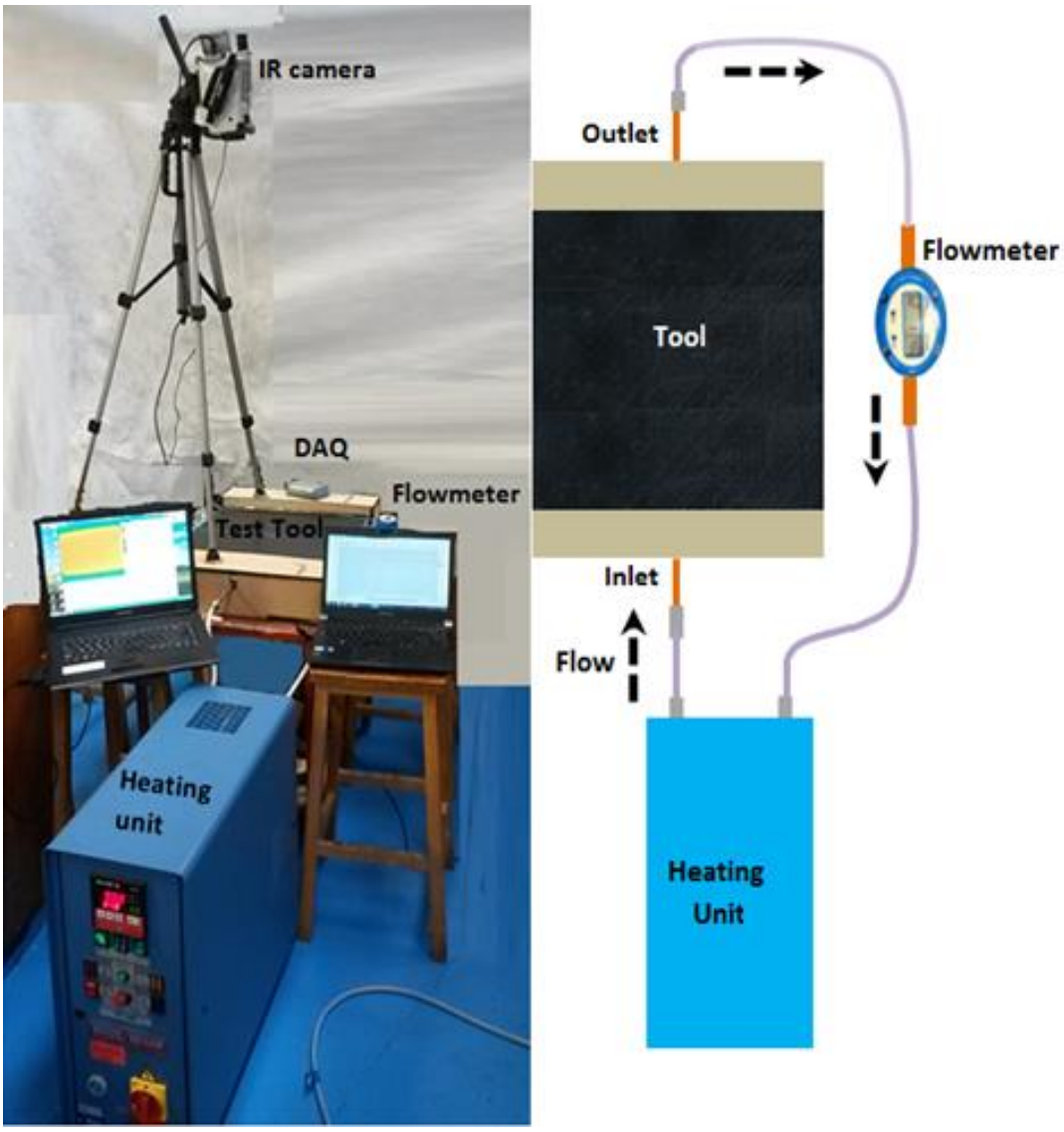

Figure 9 Test rig construction

5.2 Measurement apparatus

5.2.1 Emissivity of the CFRP laminate for thermal camera

Measurement of temperature by the thermal camera depends on emitted infra-red radiation, therefore the most important parameter is emissivity, which represents the ability of the object to absorb, transmit and emit infrared energy, compared to a perfect black body at the same temperature. The reference method, as described in ISO 18434-1, is used to determine the emissivity of the CFRP surface of the experimental tool. The method is suitable for objects with temperatures up to 260°C and based on applying a reference black material of known emissivity to determine that of the desired material (T&PI, 2014). The emissivity test procedure involves measuring the tool face temperature, with and without the reference (black PVC tape -Wilko BS3924, emissivity is 0.95); the comparison is shown in Figure 10. An emissivity of 0.94 was determined for the CFRP tool face, giving a maximum uncertainty in temperature measurement with the thermal camera of about 0.2°C.

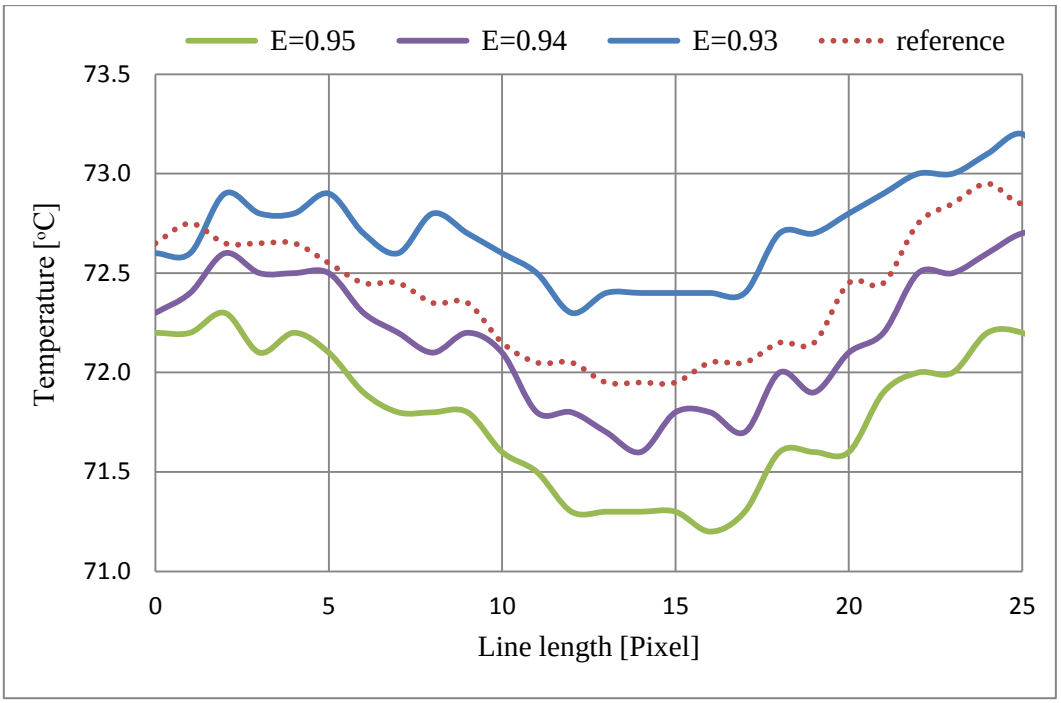

Figure 10 Temperature distributions along a specified line over the tool face, with and without PVC tape.

5.2.2 Error estimation of thermocouple measurements

The flexible K type thermocouples were made by Labfacility. Each has a copper disc of 6.5 mm diameter and 0.3 mm thick welded to the hot junction. The measurement range of the thermocouples is from 0ºC to 200ºC with a tolerance of ±2.5ºC according to IEC 584-2 specification (formerly BS4937:1983). The thermocouples are tested experimentally, to estimate the accuracy compared to the thermal camera and oven (Huber, 2013). Results show a systematic error of about 2ºC in the thermocouples which read lower than the others, but this is within their specified tolerance.

5.2.3 Calibration of the Flowmeter

The liquid Vortex OVAL Eggs Delta flowmeter (model FLM21-10PCW from Icenta) was calibrated gravimetrically and its measurement accuracy confirmed (Baker, 2000; Satterfield, 2013).

5.3 Experimental test

Initial tests found that the cold water, during tool heating, needs about 10 min to reach 90°C from the ambient (initial) temperature of 17°C, as shown in Figure 11. Also the slowest corner on the tool face reaches the target temperature of 81ºC after about 18 min. Therefore subsequent experiments were performed by pumping hot water, at 90°C, into the tool channel, as assumed in the numerical analysis (Section 4.2).

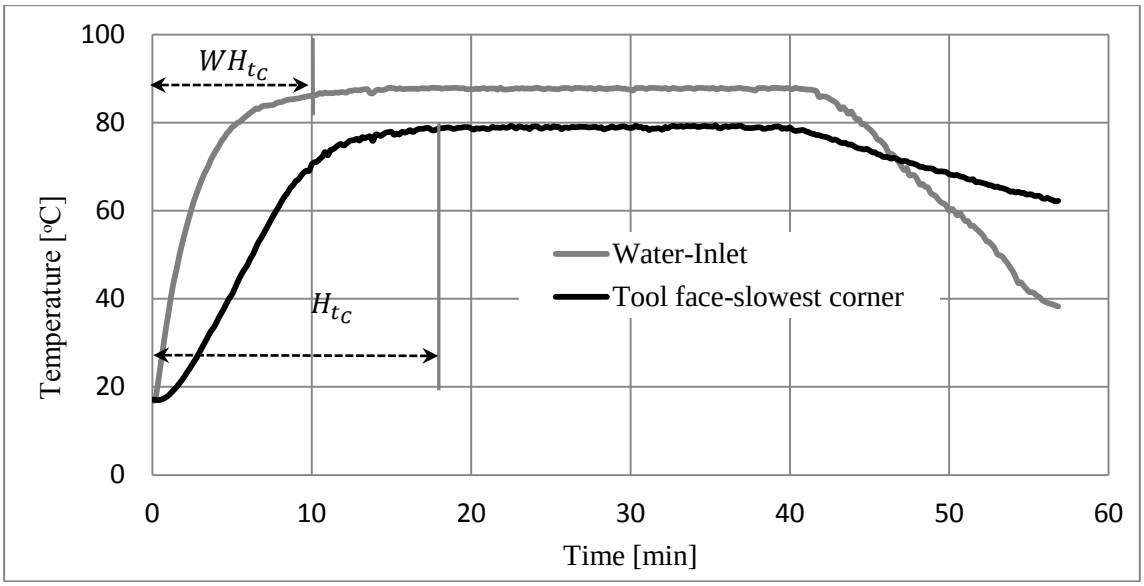

Figure 11 Temperature curves during heating of the cold water and tool.

As shown in Figure 12, hot water also requires 2.8 min to reach 90°C due to the delay in connecting the heating unit with the tool and also refilling the heating unit with extra water to replace water spilled during connection.

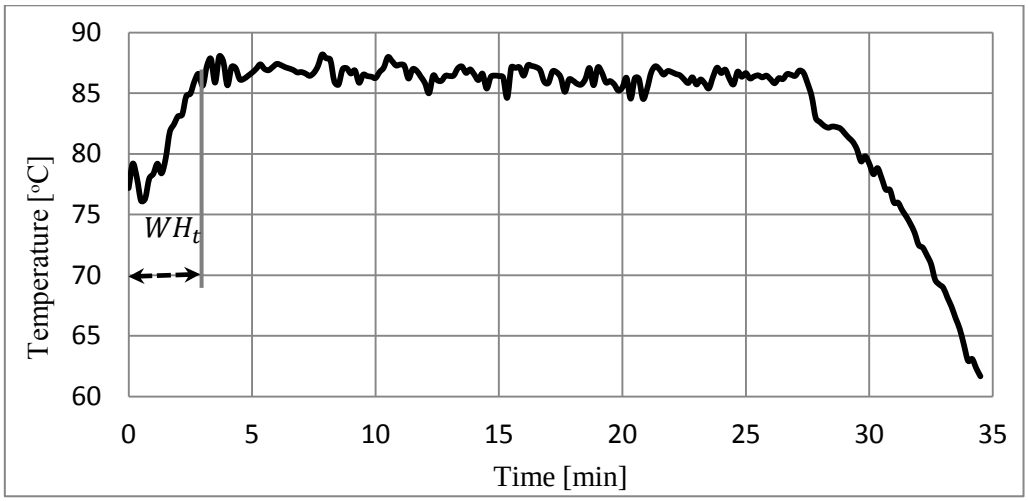

Figure 12 Temperature of the hot water at the inlet during tool heating.

Figure 13 presents the temperature-time curves of points at the centre and the slowest corner of the tool surface as measured by the thermocouples and the thermal camera. The temperature measured by the thermocouples is lower than that by the thermal camera due to the systematic error mentioned above (Section 5.2.2). It is concluded that the heating time (time required for the slowest corner to reach the target temperature) with hot water is 12.8 min; the actual value is 10 min if the delay time of 2.8 min as the water heats up to 90°C is deducted.

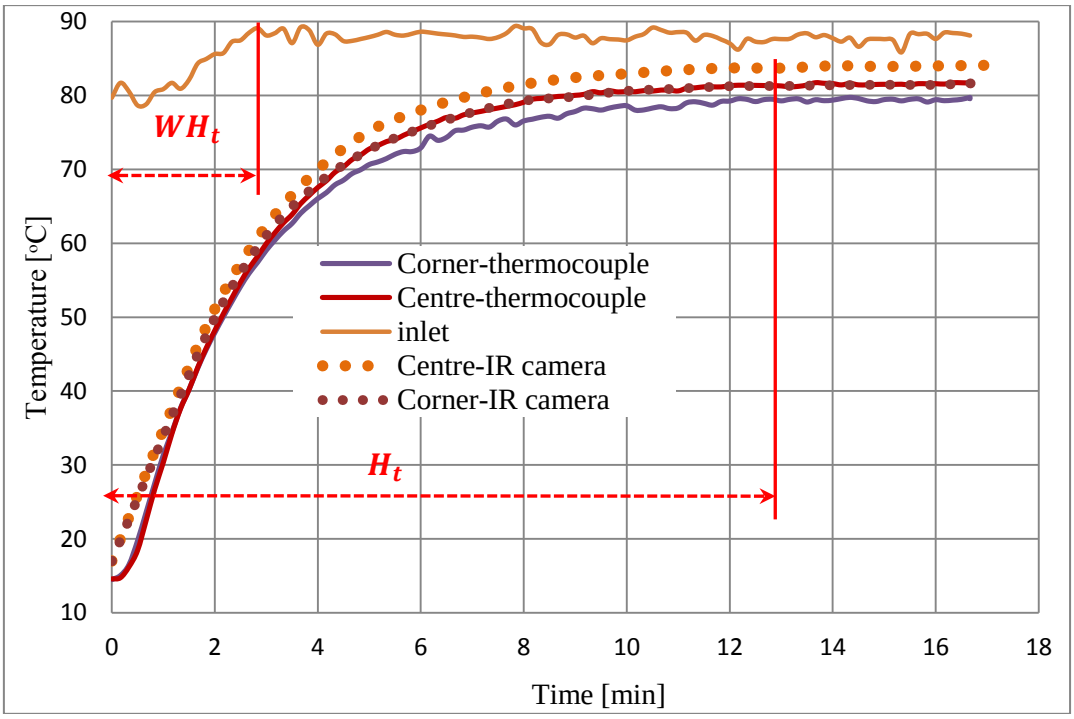

Figure 13 Experimental temperature curves of the centre and corner of the tool face, when hot water is pumped.

The image of the experimental tool face captured by the thermal camera with emissivity set at 0.94, after 10 min heating, is illustrated in Figure 14. The black rectangular area is used by the camera's MicroSpec software to calculate area-weighted average temperature (Table 5).

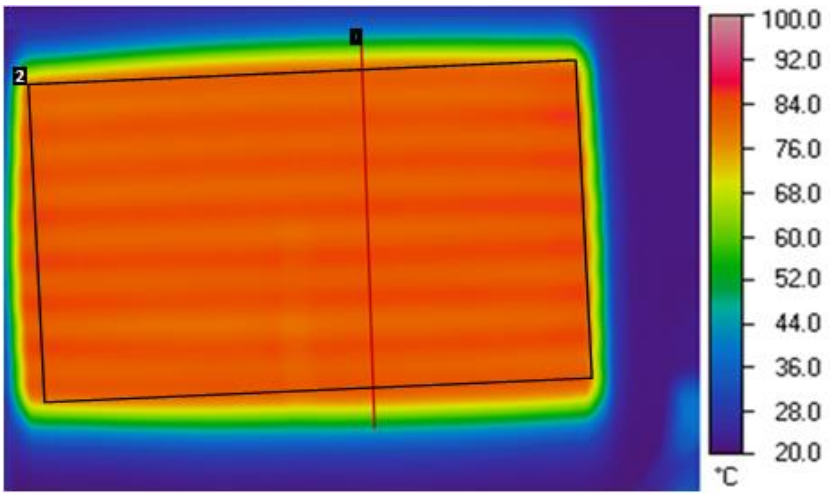

Figure 14 Experimental thermal image of the tool face after 10 min heating, emissivity = 0.94.

Temperature distributions along the width of the tool face (the red line in Figure 14), are extracted by the MicroSpec software at different times and plotted in Figure 15A. A temperature decrease can be seen at the both edges of the heated area. Figure 15B illustrates the temperature distribution along the half width of the experimental tool.

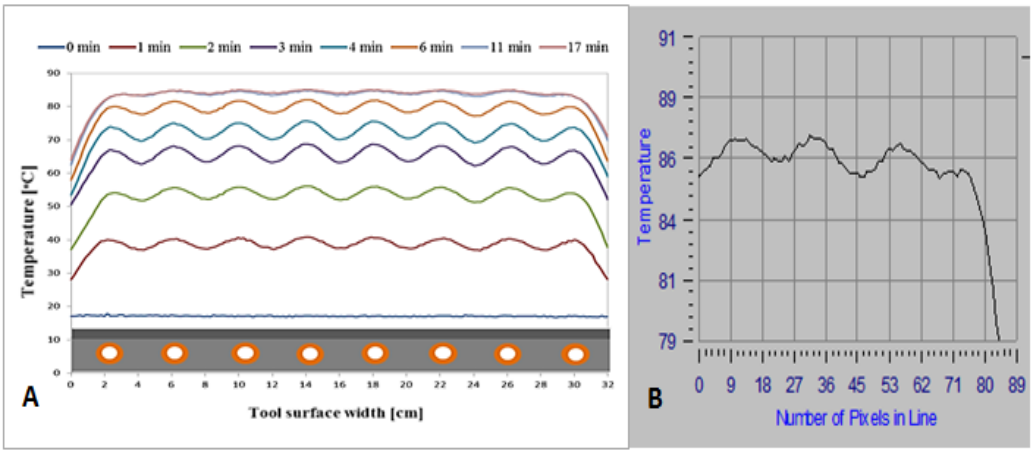

Figure 15 Experimental temperature distribution on the tool surface. **A**: along the width of the tool at different heating times. **B**: along a half width of the tool face, after 10 min heating, plotted by the MicroSpec software.

5.4 Experimental verification

In order to facilitate their comparison, the numerical and experimental results are plotted or listed together as follows:

- The numerical and practical thermal images of the experimental tool face are shown together in Figure 16 and show that the temperature distributions resulted largely similar.

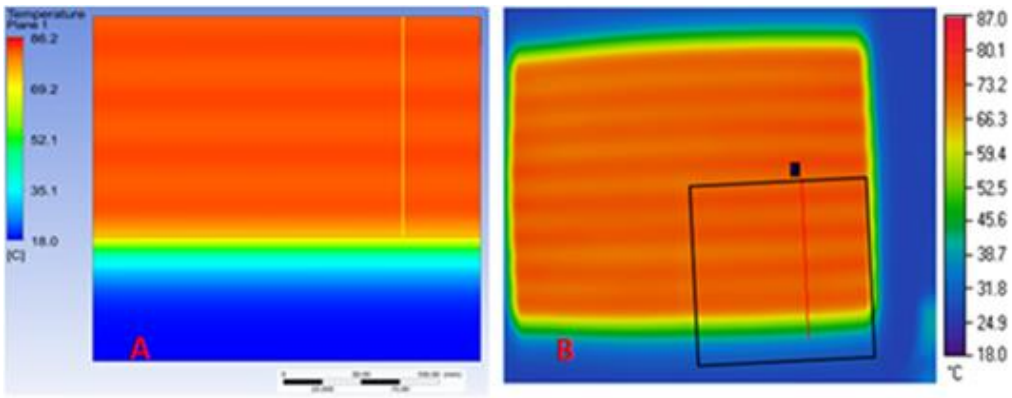

Figure 16 Numerical and experimental thermal images of the tool surface at the corresponding heating times. **A**: quarter of the tool model surface, numerically. **B**: total tool surface, experimentally by thermal camera.

- The experimental and numerical isotherm profiles, along a half width of the tool surface (lines shown in Figure 16), are presented together in Figure 17. The maximum difference between the numerical and practical temperatures over the tool face varies between 0.3 and 1°C, which shows a good agreement between the two results. The temperature decrease at the edge is similar for both methods, although the width of the experimental profile is larger by about 6 mm.

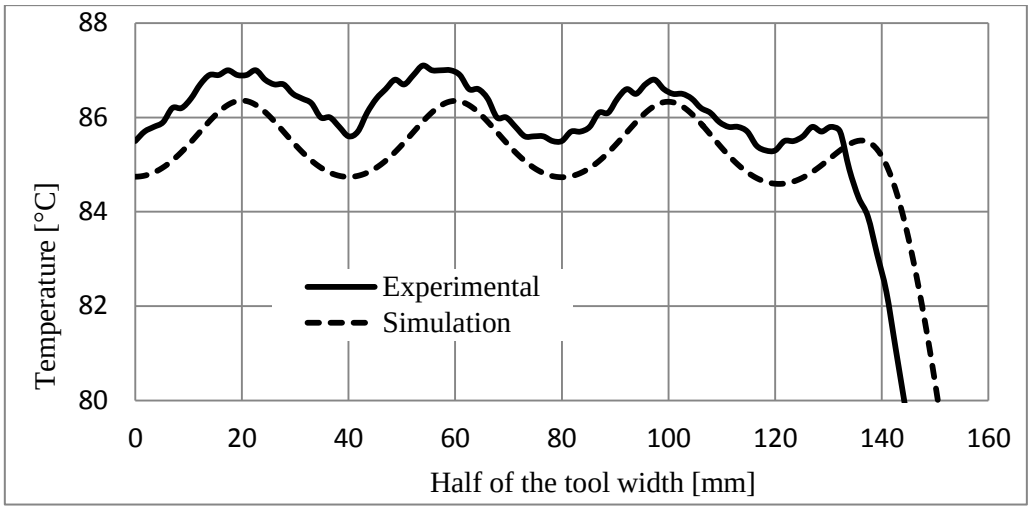

Figure 17 Experimental and numerical temperature distribution along a half width of tool face, at the same heating times

- The numerical and experimental transient temperature curves of the slowest corner of the tool face are plotted in Figure 18. They show that the experimental heating time is higher due to the delay in the hot water in reaching the desired maximum temperature of 90°C. The thermocouples measurements did not match those of the thermal camera due to the systematic error estimation (Section 5.2.2).

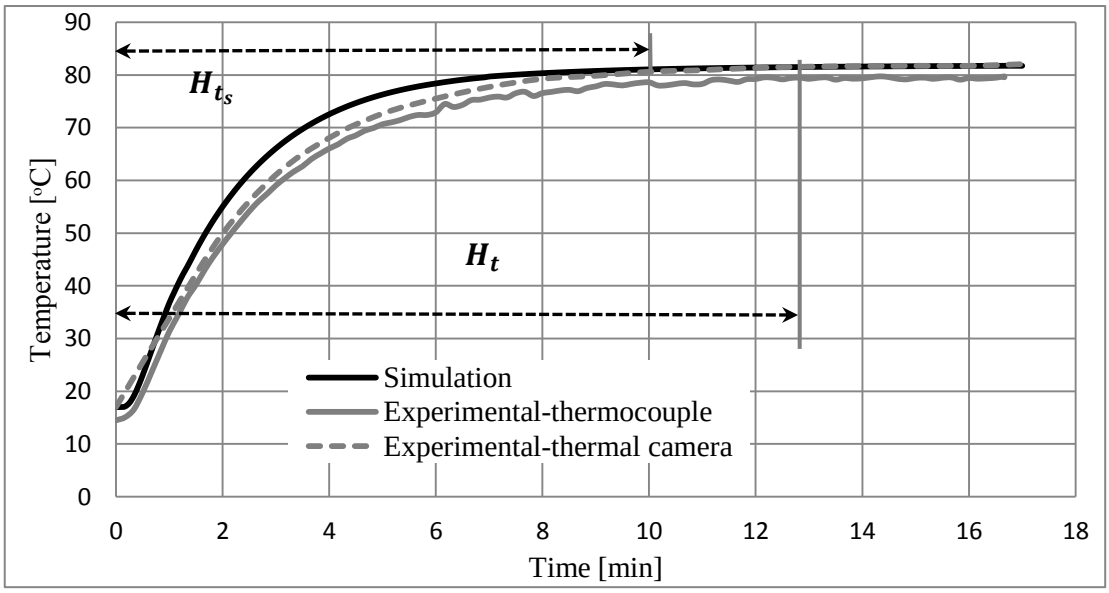

Figure 18 Experimental and numerical temperature curves at the slowest tool corner.

The various thermal results are summarised in Table 5, for comparison and further validation. The table also includes the predicted values of the both optimal designs and their limits (the first illustrated in Section 3.1, while the second was found to be parallel layout, rectangular tube profile and 50 mm channel separation, considering the response variable of temperature variation between T_{ave} and target temperature of 81°C) that were obtained in the previous optimisation study (Abdalrahman *et al.*, (2014).

Table 5 Numerical and experimental results and predicted optimal values. Tool mass is 6.3 kg and target temperature is 81ºC.

Factors of comparison	Units	Simulation (case 1)	Experimental	Predicted Optimal values with tolerances
Heating time	min	10.3	10	-
Heating time per unit mass	min/kg	1.6	1.59	1.4 ±0.77 (For the first optimal design)
Area average temperature	°C	84.6	84.9	
Temperature variation over the tool face	°C	3.6	3.9	4.7 ±0.4 (For the first optimal design)
Width of thermal gradient zone from each edge	mm	12	17	-
Temperature decrease at the tool edge.	°C	11	16	-
Temperature difference between the outer and inner channels	°C	1	1.3	-
Temperature difference between the points over the inner channels and their between	°C	1.6	1.7	-

The good agreement between experimental and numerical results confirms that the numerical analysis is successful in defining the thermal performance of the composite tooling and also that appropriate boundary conditions and material properties were used for the simulation. The experimental results also confirm that the predicted optimal design of heating time per unit mass, illustrated in Section 3.1, falls within the predicted limits set by the confidence interval in previous study.

The experimental heating time of the tool (with the amended optimal design) is slightly larger than the theoretical values, while heating time is inversely proportional to surface average area temperature (T_{ave}), as concluded by Abdalrahman et al. (2014). Accordingly T_{ave} over the face of the tool will be lower than the optimal design as will the temperature variation (difference between T_{ave} and target temperature of 81ºC). This explains why the temperature variation over the experimental tool is lower than that predicted for the aforementioned second optimal design.

The channel distance and low thermal conductivity of the existing materials are the main causes of temperature variation perpendicular to the channel alignment, because the heat requires more time (higher than the target heating time) to spread uniformly through the tool material.

6 Conclusion

An experimental tool was manufactured according to an optimal design predicted theoretically in a previous study, with some amendments to facilitate the production and monitoring of thermal performance. The thermal properties of the constituent tool materials and boundary conditions were measured experimentally, for use in a numerical simulation. The experimental tool is also tested practically to verify the numerical results. Good agreement between the experimental and numerical results was found, which confirms the suitability of simulation in optimising heating performance and also the validity of the boundary conditions and material properties. Experimental results also confirmed that the optimal design of the integrally water-heated tool falls within the predicted limits set by the confidence interval in (Abdalrahman *et al.*, 2014).

Acknowledgements

The authors would like to acknowledge financial support from the Ministry of Higher Education and Scientific Research of the Republic of Iraq. Particular thanks are given to Polytechnic University of Slemani and the University of Plymouth for their support. Dr Richard Cullen, Dr Robert Allen, Terry Richards, Kev Solman and Andy Arnold (all Plymouth University) assisted with various aspects of the experimental work. Dr Hom Dhakal (University of Portsmouth) assisted with thermal testing.

References

Abdalrahman, R., Grove, S., Kyte, A. & Rizvi, M. J. (2014) 'Numerical simulation and design optimization of an integrally-heated tool for composite manufacturing'. *Materials & Design*, 64 (0). pp 477-489.

Arney, M. W., Grove, S. M., Progoulakis, I., Searle, T. J., Short, D., Spooner, J. & Summerscales, J. (2004) 'Integrally-heated tooling for the manufacture of fibre-reinforced composites', *Proceedings of Composites Processing, CPA, April 2004*. Bromsgrove.

ASTM D792-13 (2013) 'Standard Test Methods for Density and Specific Gravity (Relative Density) of Plastics by Displacement'. *ASTM International Book of Standards*, 8.1 (PA).

Baker, R. C. (2000) *Flow Measurement Handbook: Industrial Designs, Operating Principles, Performance and Applications.* Cambridge: Cambridge University Press.

Baril-Gosselin, S. (2013) *Improving Integrally Heated Composite Tooling Through Cold Sprayed Copper Coatings and Heat Transfer Simulations*. University of Ottawa.

Black, S. (2010b) *Mold heating study proves pressurized water system.* High-Performance Composites. Available at: http://www.compositesworld.com/articles/mold-heating-study-proves-pressurized-water-system (Accessed: 22/06/2015).

Black, S. (2011) 'Tooling for Composites: Evolutionary Trajectory'. *High Performance Composites*, (July), [Online]. Available at: http://www.compositesworld.com/articles/tooling-for-composites-evolutionary-trajectory (Accessed: 06/06/2012).

BS 7658 (1995) 'Carbon fibre -Detemunation of size content'. *Part 3*, British Standards Institution, pp 12.

Campbell, F. C. (2004) *Manfacturing processes for advanced composites* New York: Elsevier

Cassel, B., Salamon, A., Sahle-Demessie, E., Zhao, A. & Gagliardi, N. (2012) 'Improved Hyper DSC Method to Determine Specific Heat Capacity of Nanocomposites and Probe for High-Temperature Devitrification'. [Online]. Available at: http://www.perkinelmer.co.uk/PDFs/Downloads/APP_NanocompositesHyperDSC.pdf.

Davis, J. R. (2001) *Copper and copper alloys.* Materials Park, OH : ASM International

Ding, Y., Chiu, W. K., Liu, X. L. & Whittingham, B. (2001) 'Modelling of thermal response of oil-heated tools due to different flow rates for the manufacture of composite structures'. *Composite Structures*, 54 (4). pp 477-488.

East Coast (2013) *Aluminium powder-250 mesh.* Available at: http://www.ecfibreglasssupplies.co.uk/p-817-aluminium-powder-250-mesh.aspx (Accessed: 06/02/2014).

Gallagher, D. P. (2012) *Through-Thickness Thermal Conductivity Improvement Of Carbon Fiber Reinforced Composites By Using A Heterogeneously Structured Resin Matrix* Master Thesis. The Florida State University.

Han, S. & Chung, D. (2011) 'Increasing the through-thickness thermal conductivity of carbon fiber polymer–matrix composite by curing pressure increase and filler incorporation'. *Composites Science and Technology*, 71 (16). pp 1944-1952.

Han, S., Lin, J. T., Yamada, Y. & Chung, D. (2008) 'Enhancing the thermal conductivity and compressive modulus of carbon fiber polymer–matrix composites in the through-thickness direction by nanostructuring the interlaminar interface with carbon black'. *Carbon*, 46 (7). pp 1060-1071.

Holman, J. P. (2002) *Heat Transfer.* 9th edn. New York: McGaw-Hill.

Huber, R. (2013) 'Temperature Measurement with Thermocouples: Application Note'. *OSRAM Opto Semiconductors*, pp 1-13.

Incropera, F. & DeWitt, D. (1996) *Fundamentals of heat and mass transfer* Chichester : Wiley, 1996.

Instruction LTI/CHEM/037 (2003) 'Composite Fibre/Resin/Void Content Using Matrix Digestion Method'. *Issue 1, GKN Aerospace Services, Cowes, UK*,

Konzelmann, S., Hoffmann, C., Merte, R. & Peier, D. (2008) 'Thermal and electrical properties of aluminum nitride filled epoxy-resin compound'. *Dielectrics and Electrical Insulation, IEEE Transactions on*, 15 (2). pp 327-333.

Kruckenberg, T. M. & Paton, R. (1998) *Resin transfer moulding for aerospace structures.* Great Britain: Kluwer Academic

Marsh, G. (2003) 'Mould tool heating – the oven-free alternative'. *Reinforced Plastics*, 47 (11). pp 38-41.

Mason, K. (2006) 'Autoclave Quality outside the autoclave'. *High-Performance Composites*, (March), [Online]. Available at: http://www.compositesworld.com/articles/autoclave-quality-outside-the-autoclave (Accessed: 06/06/2012).

MatWeb (2014) 'Foam Core Material '. in DataSheet *DIAB Divinycell H 160 Sandwich Core Material* MatWeb: DIAB, Inc. Available at: http://www.matweb.com/search/DataSheet.aspx?MatGUID=da57c5a813ce43b3a81d82e3600e40a4 (Accessed: 10/02/2013).

Mazumdar, S. K. (2001) *Composites manufacturing : materials, product, and process engineering.* CRC Press

Milella, E., Spena, P., Giusto, G. & Thomas, J. (2014) 'The Influence of Several Fillers on the Thermochemical and Mechanical Properties of High Performance Thermoplastic Polymers'. *ECCM16*. Seville-Spain: 22-26 June 2014.

Munson, B. R. (2010) *Fundamentals of fluid mechanics.* 6th edn. Hoboken N.J. Wiley.

Murisic, N., Pausader, B., Peschka, D. & Bertozzi, A. L. (2013) 'Dynamics of particle settling and resuspension in viscous liquid films'. *Journal of Fluid Mechanics*, 717, pp 203-231.

Murphy, J. (1998) *The reinforced plastics handbook.* 2nd edn. Elsevier Advanced Technology.

Petrykowski, K. & Fischer, J. (2012) 'A study comparing electric, oil and pressurised water heating for composite moulding'. *JEC Composites,* (75). pp 42-47.

PMC *Mold Temperature Control Effectiveness Electric Heat vs. Pressurised Water.* PMC smart solutions. Available at: http://www.single-temp.co.uk/fileadmin/downloads/PDF_Composites/PMC_Test_electric_heat_vs_water.pdf (Accessed: 05/01/2015).

Progoulakis, I. (2004) *Heated tooling for aerospace composites manufacture*. Master Thesis. University of Plymouth.

Raizenne, D., Hind, S. & Poupore, J. (2006) 'Integral heating for composite tooling', *Design, Manufacturing and Applications of Composites: Proceedings of the Sixth Joint Canada-Japan Workshop on Composites*. DEStech Publications, Inc, pp. 133.

Rosato, D. V. (2004) *Reinforced plastics handbook.* 3rd edn. New York : Elsevier

Satterfield, Z. (2013) 'Reading Centrifugal Pump Curves'. *Tech Brief*, 12 (1). pp 1-5.

Schuster, J., Heider, D., Sharp, K. & Glowania, M. (2008) 'Thermal conductivities of three-dimensionally woven fabric composites'. *Composites Science and Technology*, 68 (9). pp 2085–2091.

Schuster, J., Heider, D., Sharp, K. & Glowania, M. (2009) 'Measuring and modeling the thermal conductivities of three-dimensionally woven fabric composites'. *Mechanics of Composite Materials*, 45 (2). pp 165-174.

Scott Bader Company (2005) *Performance Resins in Composites.* Scott Bader Company Ltd: Wollaston, Wellingborough, Northamptonshire NN29 7RL.

Senthilkumar, N., Kalaichelvan, K. & Elangovan, K. (2012) 'Mechanical Behaviour of Aluminum particulate epoxy composite–Experimental study and Numerical simulation'. *International Journal of Mechanical and Materials Engineering, 7 (3),* pp 214-221.

Sicomin-Composites (2013) *Epoxy resin systems Multi purpose for composites applications.* Available at: http://www.matrix-composites.co.uk/prod-data-sheet/old/sr-8500-860x-uk.pdf (Accessed: 06/02/2014).

Sigmatex (2014) *Global Carbon Composite Solutions.* UK: Sigmatex UK Limited. Available at: http://www.sigmatex.com/technical/technical-specifications/ (Accessed: 17/06/2015).

Sloan, J. (2013) 'Pressurized Water-based mold temperature control comes to composites '. *High-Performance Composites magazine*, (January), [Online]. Available at: http://www.compositesworld.com/articles/pressurized-water-based-mold-temperature-control-comes-to-composites (Accessed: 04/04/2015).

T&PI (2014) *How to Determine Emissivity Values.* Technical Information Data Bulletin, USA: Temperature & Process Instruments Inc. Available at: http://www.tnp-instruments.com/sitebuildercontent/sitebuilderfiles/Infrared%20Thermometer%20and%20Emissivity.pdf (Accessed: 12/08/2013).

Tomlinson, W. J. & Stapley, D. (1977) 'Thermal conductivity of epoxy resin-aluminium'. *Journal of Materials Science*, 12 (8). pp 1689-1690.

Walczyk, D. & Kuppers, J. (2012) 'Thermal press curing of advanced thermoset composite laminate parts'. *Composites Part A: Applied Science and Manufacturing*, 43 (4). pp 635-646.

Yao, D., Chen, S.-C. & Kim, B. H. (2008) 'Rapid thermal cycling of injection molds: An overview on technical approaches and applications'. *Advances in Polymer Technology*, 27 (4). pp 233-255.

Yoo, S. & Walczyk, D. F. (2007) 'A Preliminary Study of Sealing and Heat Transfer Performance of Conformal Channels and Cooling Fins in Laminated Tooling '. *Journal of Manufacturing Science and Engineering-transactions of The Asme*, 129 (2). pp 388-399.

Zhou, W. & Yu, D. (2010) 'Thermal and dielectric properties of the aluminum particle/epoxy resin composites'. *Journal of Applied Polymer Science*, 118 (6). pp 3156-3166.

Zhu, B. L., Wang, J., Ma, J., Wu, J., Yung, K. C. & Xie, C. S. (2013) 'Preparation and properties of aluminum nitride-filled epoxy composites: Effect of filler characteristics and composite processing conditions'. *Journal of Applied Polymer Science*, 127 (5). pp 3456-3466.

Zweben, C. (1998) 'Overview of advanced composites for thermal management', *Advanced Packaging Materials, 1998. Proceedings. 1998 4th International Symposium on*. 15-18 Mar 1998. pp. 183-197.